Semiconductor Science and Technology

Laplace DLTS study of the fine structure and metastability of the radiation-induced E3 defect level in GaAs

To cite this article before publication: Fatemeh Taghizadeh *et al* 2018 *Semicond. Sci. Technol.* in press https://doi.org/10.1088/1361-6641/aae9a8

Laplace DLTS study of the fine structure and metastability of the radiation-induced E3 defect level in GaAs

F. Taghizadeh, K. Ostvar, F. D. Auret and W. E. Meyer

Department of Physics, University of Pretoria, Private Bag X20, Hatfield 0028, Pretoria

Abstract

In this paper we used high resolution Laplace Deep-Level Transient Spectroscopy (DLTS) to study the electrical properties of the E3 defect family introduced in GaAs by MeV electron irradiation. We found that the peak conventionally referred to as the E3 contained 3 components which we labelled E3a, E3b and E3c, with E3a being the most prominent component. The activation energy of E3a for different carrier densities varied between 0.36 eV and 0.375 eV. From dopant dependent introduction rate measurements, we found that the introduction rates of the E3a and E3b defect did not depend on doping density. However, the E3c concentration increased with increasing carrier density. Furthermore, the E3c was found to be metastable: it was reversibly removed during minority carrier injection at low temperatures and re-introduced by annealing above 160 K under zero bias. Interestingly, annealing measurements revealed that, of the three components, the E3b annealed first at around 500 K while both the other components annealed together at a higher temperature of 525 K. By comparing our results with previous studies, we concluded that the origin of E3a is $V_{As,}$ E3b is As_i and E3c is $V_{Ga} - Si_{Ga}$.

- Corresponding author email: F.Taghizadeh@tuks.co.za

- Keywords: Electron irradiation induced defects in GaAs; Laplace Deep-Level Transient Spectroscopy, Introduction rate; Metastability; defect annealing, Phonon-assisted tunnelling

1. INTRODUCTION

Deep-level transient spectroscopy (DLTS) was introduced by Lang in 1974 [1]. This powerful technique is used to analyze deep level defects in semiconductors [1], [2]. The major shortcomings of DLTS are the lack of structural information and limited spectral resolution [3]. Laplace deep-level transient spectroscopy [LDLTS] was introduced by Dobaczewski and Peaker [3] to overcome the spectral resolution shortcoming of DLTS. This technique has a higher resolution than DLTS and is capable of separating defects which have very similar carrier emission rates.

Deep- and shallow-level defects significantly affect the electrical properties of semiconductors. These defects can be introduced during crystal growth or processing steps such as ion implantation, metallization, etching and annealing [4]. In order to fully understand the origin and effect of a defect, factors should be considered include: deep-level introduction method, doping density and temperature, crystal growth method and defect annealing dynamics.

Gallium arsenide (GaAs) is a III-V, direct band gap semiconductor. It has high electron mobility and a moderately wide band gap (1.424 eV). Because of these properties it is a suitable candidate for high frequency applications such as satellite communications and microwave point-to-point links. In this article, the aim is to investigate the E3 defect introduced in epitaxially-grown gallium arsenide by MeV electron irradiation.

Since the first detection of the E1, E2 and E3 radiation-induced defect levels in GaAs by Lang *et al.* in 1977 [5], there have been many speculations regarding their possible nature and origin. Lang *et al.* [5] concluded that the origins of the E1 and E2 are Ga_i or As_{Ga}, with which Farmer *et al*. [6] agreed. However, the results of Pons *et al.* [7] and Stievenard [8] show that both the E1 and E2 are due to V_{As} while in 2015 Schultz [9] used DFT calculations to prove that these two levels are due to the divacancy. From DLTS results and Hall measurements, Lang [5] and Farmer [6] both proposed that E3 is a V_{Ga}. However, from a study combining theory and DLTS, Murawala *et al.* [10] concluded that E3 is a V_{As}. This conclusion was also recently supported by Schultz using DFT (using LDA and PBE) [9]. On the other hand, several authors proposed that

the E3 consists of defect pairs: Pons *et al.*[7] and Stievenard [8] using EPR found evidence for the $V_{As} - As_i$, and Bardeleben *et al.* [11] using EPR for the $As_{Ga} - V_{As}$. The E3 was also proposed to be the antisite As_{Ga} by Schick *et al* [12].

For this work, GaAs samples were irradiated by beta radiation emanating from ^{90}Sr to introduce point defects. The MeV electrons from this source have sufficient kinetic energy to displace at least one single atom [7]. Using L-DLTS, we found that the E3 level observed in conventional DLTS actually consists of three defect levels with distinct properties. These results can be used to reconcile apparently conflicting results regarding the origin of the E3 level.

2. EXPERIMENTAL PROCEDURES

For this experiment we used small rectangularly shaped pieces of n-type OMVPE-grown GaAs on n^{++} GaAs substrates. GaAs was used from various wafers with different silicon doping densities with free carrier densities of 7.1×10^{14} cm^{-3}, 1.9×10^{15} cm^{-3} and 1.0×10^{16} cm^{-3}. The samples were degreased by boiling in trichloroethylene for 3 minutes and then boiled in isopropanol for another 3 minutes. After that, the pieces were rinsed with deionized water, then, for chemical etching, the samples were dipped in a solution of H_2O [100%]: H_2O_2 [50%]: NH_4OH [25%] with (100:1:3) volume ratios for 60 seconds. Hereafter the samples were again rinsed in deionized water and then dipped in a solution of 6 mol dm^{-3} HCl for 60 seconds and finally rinsed in deionized water and blow dried by nitrogen gas. Next, the samples were positioned in a resistive evaporation chamber to deposit a layered ohmic contact (Ni (5 nm), Au-Ge (145 nm), and Ni (50 nm)) on the back surface of each sample. The deposited ohmic contacts were annealed at 450°C for 2 minutes in an Ar-filled environment. The samples were cleaned again to prepare them for Schottky contact deposition. For second cleaning, we skipped the dipping in H_2O: H_2O_2: NH_4OH. The samples were positioned in the same deposition chamber and 0.6 mm diameter Au Schottky contacts were deposited on the epitaxially-grown surface of the samples through a metal contact mask.

After contact formation the samples were individually subjected to electron irradiation using ^{90}Sr source, with each sample being irradiated for specific durations, depending on their free carrier densities. This radiation was chosen so as to not affect the carrier densities at room temperature. Note that all the measure radiation induced defect are empty at room temperature because of their energy levels position in the band gap. The aim of the experiments was to confirm the existence of the E3 defect in each sample. This was achieved by using conventional DLTS. After the confirmation step, E3 was characterized using Laplace DLTS. The aim of this was to detect the finer structure of the E3 and characterize its formation and behavior in each sample. The results were compared against each other in an attempt to determine the influence of the duration of the irradiation as well as the effect of the carrier density on the E3 center.

Electric field measurements of the E3a, the most prominent component of the E3, were done for 3 different carrier densities. The field effect data was analyzed according to the Poole-Frenkel model [13] as well as the phonon assisted tunneling model of Ganichev *et al.* [13], [14] from which the tunneling time could be determined. In order to gain insight into the origin of the different components, the introduction rates, annealing properties, capture cross section and possible metastability of the individual components of the E3 defect were investigated.

3. RESULTS AND DISCUSSION

Figure 1 shows the DLTS and Laplace DLTS spectrum of three different carrier densities. DLTS spectrum was recorded over the temperature range 20 – 300 K as shown in Figure 1(b) and the Laplace DLTS spectrum of the E3 defect at 205 K is shown in Figure 1(a). The DLTS spectrum demonstrates the presence of three prominent peaks: E1, E2 and E3, which were spaced far apart in temperature at approximately 30 K, 70 K and 200 K, indicating that the energy levels are spaced well apart in the band gap. From the conventional DLTS spectrum it seems that the E3 is a single peak (albeit slightly broad and with some asymmetry for the 1.0×10^{16} cm^{-3} doped GaAs). However, by using Laplace DLTS, it was clear that the E3 comprised of 3 different individual components which we labeled E3a, E3b and E3c. The properties of the three defects are

listed in Table I. In the DLTS graph (Figure 1(a)) we observed the comparison between the three different carrier densities. The E3 peak for the higher carrier density is shifted to the left, it is broader and it is asymmetric towards lower temperature side. The Laplace DLTS spectrum of the E3 shows that the relative amplitude of the E3c peak is enhanced at higher carrier densities, thereby explaining the shift and broadening observed in the conventional DLTS spectrum.

The Arrhenius plots of the E3 and its components (E3a, E3b and E3c) in three samples with different free carrier densities (7.1×10^{14} cm^{-3}, 1.9×10^{15} cm^{-3} and 1.0×10^{16} cm^{-3}) were plotted and showed three distinct levels, as shown in Figure 2. The activation energies for all three components were close to activation energies of the E3 reported in literature. Note that the activation energy for all three components decreased with increasing free carrier density, i.e. for E3a, 0.383 eV, 0.372 eV and 0.360eV for 7.1×10^{14} cm^{-3}, 1.9×10^{15} cm^{-3} and 1.0×10^{16} cm^{-3} free carrier concentration, respectively, but the activation energies of E3b and E3c results for 7.1×10^{14} cm^{-3} are with a $\pm$ 0.01 eV error bar which is due to lower concentration of these defects compared with the higher carrier densities.

To investigate whether or not the E3 defects depended on the Si dopant, we did introduction rate measurements of the main component, E3a, for three different carrier densities. Figure 3 shows the results, and it is clear that the introduction rate was the same for all the free carrier densities. This indicates that the E3a defect does not involve a dopant atom, in this case Si. We found the introduction rate of the E3a in our samples was 0.42 cm^{-1}, which agrees with the value of 0.4 cm^{-1} found by Pons [7]. Note that the E3b and E3c components for the lower doping density GaAs were too small to allow for an accurate measurement of their introduction rates as function of doping density.

Figure 4 shows Laplace DLTS spectra of samples with different carrier densities. For each carrier density, three different spectra are shown: before minority carrier injection, after injection and subtracted from each other. The principles of minority carrier injection were first explained by Auret *et al*.[15] and it was applied for the E3 defects in GaAs [16]. Firstly, from the graphs we see that the relative concentration of the E3c increased with increasing carrier density. Secondly, before injection the spectrum consisted of all 3

components of the E3 defect. However, after injection the E3c was reversibly removed and the spectrum consisted only of E3a and E3b. The injected spectrum was recorded after subjecting the diode to minority carrier injection pulses at low temperatures (90 – 120K). For the re-introduction of the E3c, the sample was heated to above 160 K under zero bias. The subtracted spectrum shows only the E3c. These processes were reproducible and indicate that the E3c is metastable. This phenomenon has been observed previously [17], and been ascribed to charge state controlled metastability involving hole capture and emission.

Electric field dependence of the main E3 component, E3a, was measured for 3 different carrier densities to distinguish between Poole-Frenkel (emission rate proportional to the square root of the electric field) and phonon assisted tunneling (emission rate proportional to the square of the electric field) [13], [14]. From Figure 5 it is clear that the field enhanced emission of carriers is best described by phonon assisted tunneling, with all 3 different carrier densities providing consistent results. Figure 6 (a) shows the graphs of emission rate vs. the square of the electric field for different temperatures (200 K, 205 K, 210 K, 215 K and 220 K) as well as the tunneling time as a function of 1000/*T*. It is clear that the linear relationship between emission rate and electric field squared is valid over a wide temperature range.

The model by Ganichev and Prettl [18] describes the phonon assisted tunneling in terms of the tunneling time of an electron through the potential well of the defect:

$$e(E) = e_0\, exp(\frac{\tau_2^3 e^2 E^2}{3m^* \hbar}) \quad (1)$$

In this equation τ_2 is the tunneling time, E is the electric field strength, m^* is the effective mass of an electron and $\hbar$ is the Planck constant. We measured the tunneling time according to this model and Figure 6 (b), and it was found to be given by

$$\tau_2 = \frac{81000}{T} + 234\ (fs) \quad (2)$$

True capture cross-section measurements of E3a were done for two different carrier densities (1.9×10^{15} and 1.0×10^{16}) cm^{-3} as shown in Figure 7. The DLTS signal after application of a filling pulse of length t_p, may be described by [19]

$$S(t_p) = S_{inf}[1 - exp\left(\frac{t_p}{\tau_c}\right)] \quad (3)$$

here S_{inf} is the magnitude of the DLTS signal observed after a filling pulse sufficiently long to fill all the defects and τ_c is the time constant of the capture process given by

$$\tau_c = \sigma N_d v_{th} \quad (4)$$

where σ is the capture cross section, N_d is the free carrier density and v_{th} is the thermal velocity of the carriers [19]. It follows that σ may be determined from the slope of the plot shown in Figure 7:

$$\sigma = 2.3\ slope/N_D v_{th}. \quad (5)$$

Calculations using Eqn. 5, with experimentally determined slopes and values of N_D, show that the capture cross section for material with a free carrier concentration of 1.0×10^{16} cm^{-3} is about a factor of three lower than that with 1.9×10^{15} cm^{-3} (3.1×10^{-17} cm^2 *vs.* 1.0×10^{-16} cm^2).

The temperature dependence of the capture cross section may be explained by the existence of a capture barrier, ΔE, so that the capture cross section as a function of the temperature is given by [19]

$$\sigma(T) = \sigma_\infty e^{\frac{-\Delta E}{kT}} \quad (6)$$

where k is the Boltzmann constant and T is the temperature. The capture cross section for samples with a carrier density of 1.0×10^{16} cm^{-3} and 1.9×10^{15} cm^{-3} were measured at different temperatures and are used in Figure 8 to calculate the capture barriers. As shown in Figure 8, the capture barrier for 1.9×10^{15} cm^{-3} is 0.052 eV and for 1.0×10^{16} cm^{-3} is 0.090 eV. Thus, when applying Equation 6 to our results, the capture barrier for higher carrier densities is higher than for lower carrier densities.

Figure 9 demonstrates the effect of annealing on the E3 defect. The annealing measurements were done for the sample with a carrier density of 1.0×10^{16} cm^{-3}. As can be seen, the E3b defect annealed out before the other two at 500K. E3a and E3c annealed out simultaneously at 525K. This indicates that the E3b defect is structurally different from the others.

In summary, we found that the E3 is not a single defect but rather consists of three separate levels (E3a, E3b and E3c). The activation energies and apparent capture cross sections were calculated for defects in 1.0×10^{16}

cm^{-3} doped GaAs. Results from introduction rate studies indicate that the concentration of E3a and E3b is independent of the doping density and hence these defects do not involve dopant atoms. For E3c the results suggest that this component is highly dependent on carrier density. We therefore conclude that the E3c defect involves a Si dopant atom. In addition, the E3c was found to be metastable. Furthermore, results from annealing profiles for all three components show that the E3b annealed out at 500 K and the E3a and E3c annealed out at 525 K. From this, we conclude that the three components of the E3 defect are due to three structurally different defects that coincidently happen to have similar emission rates. This might explain why there is so much uncertainly in the literature about the origin of the E3. Perhaps the most interesting proposal was by Bondarenko *et al.* [20] who deduced from positron annihilation and Hall measurements that in Si-doped GaAs, E3 may be $V_{Ga} - Si_{Ga}$. This proposed defect could well be our E3c of which we have shown that the concentration is directly proportional to the Si doping concentration. E3a is the most prominent component of E3 and may therefore be the V_{As} which Bondarenko *et al*. [20] predicted to form in undoped GaAs. The latest reports regarding the E3 origin by Schultz [9] supports that E3 is $V_{As.}$ According to Stievenard *et al.* [8] the E3b can be As_i, as they mentioned E3 is a $V_{As} - As_i$ and the As_i was found to anneal out earlier (around 493 K) than V_{As} (around 523 K), then we can conclude that E3b is As_i. The annealing temperature of the E3a is further support for the E3a being due to the V_{As}.

4. CONCLUSIONS

DLTS spectra recorded between 20 K and 300 K show the presence of the E1, E2 and E3 defects in electron irradiated n-type GaAs. By using Laplace DLTS we have found that the E3 is not a single peak but consists of three individual components (E3a, E3b and E3c) with different structures. For the 1.0×10^{16} cm^{-3} doped GaAs the activation energies were 0.360 eV, 0.392 eV and 0.335 eV, respectively, and their apparent capture cross sections were 2.1×10^{-14} cm^2, 4.8×10^{-13} cm^2 and 6.8×10^{-14} cm^2 for E3a, E3b and E3c, respectively. Carrier density dependent introduction rate results indicate that the E3c defect involves a Si dopant atom while the E3a and E3b do not. In addition, the E3c is also metastable: it can be removed by injecting minority carriers

at low temperatures and re-introduced by heating up above 160 K under zero bias. Very important, we also observed that of the three components, the E3b annealed out first at 500 K and both the other components annealed out at 525 K. We conclude that all three components are structurally different and, by comparing the properties with results with those of other researchers, it is clear that E3a is V_{As}, E3b is As_i and E3c is $V_{Ga} - Si_{Ga}$. From the electric field measurements, we found that the field enhanced emission of carriers was well described by phonon assisted tunneling. It was found that the capture cross section of the 1.9×10^{15} cm^{-3} doped material is higher than in the 1.0×10^{16} cm^{-3} doped material.

ACKNOWLEDGMENTS

This work is based on the research supported by the National Research Foundation of South Africa under grant number 98961. Opinions, findings and conclusions or recommendations are that of the authors, and the NRF accepts no liability whatsoever in this regard. The Laplace DLTS software and hardware used here were received from L. Dobaczewski (Institute of Physics, Polish Academy of Science) and A. R. Peaker (Center for Electronic Materials Devices and Nano-structures, University of Manchester).

References:

[1] D. V. Lang, "Deep-level transient spectroscopy: A new method to characterize traps in semiconductors," *J. Appl. Phys.*, vol. 45, no. 7, pp. 3023–3032, 1974.

[2] J. L. J. Benton, "Characterization of defects in semiconductors by deep level transient spectroscopy," *J. Cryst. Growth*, vol. 106, no. 1, pp. 116–126, 1990.

[3] L. Dobaczewski, A. R. Peaker, and K. Bonde Nielsen, "Laplace-transform deep-level spectroscopy: The technique and its applications to the study of point defects in semiconductors," *J. Appl. Phys.*, vol. 96, no. 9, pp. 4689–4728, 2004.

[4] W. E. Meyer, "Digital DLTS studies on radiation induced defects in by Walter Ernst Meyer PhD (Physics) in the Faculty of Natural & Agricultural Science University of Pretoria November 2006 Supervisor : Prof F D Auret Digital DLTS studies on radiation induced defects," no. November, pp. 0–5, 2006.

[5] D. V. Lang, R. A. Logan, and L. C. Kimerling, "Identification of the defect state associated with a gallium vacancy in GaAs and AlxGa1-xAs," *Phys. Rev. B*, vol. 15, no. 10, pp. 4874–4882, May 1977.

[6] J. W. Farmer, D. C. Look, and D. C. Look, "Electron Irradiation Defects in n-type GaAs Electron-irradiation defects in n-type GaAs," *Phys. Rev. B*, vol. 21, no. 8, pp. 3389–3398, 1980.

[7] D. Pons *et al.*, "Irradiation-induced defects in GaAs," *J. Phys. C Solid State Phys.*, vol. 18, no. 20, pp. 3839–3871, Jul. 1985.

[8] D. Stievenard, X. Boddaert, J. C. Bourgoin, and H. J. von Bardeleben, "Behavior of electron-irradiation-induced defects in GaAs," *Phys. Rev. B*, vol. 41, no. 8, pp. 5271–5279, Mar. 1990.

[9] P. A. Schultz *et al.*, "The E 1– E 2 center in gallium arsenide is the divacancy," *J. Phys. Condens. Matter*, vol. 27, no. 7, p. 075801, Feb. 2015.

[10] P. A. Murawala, V. A. Singh, S. Subramanian, S. S. Chandvankar, and B. M. Arora, "Origin of an E 3 -like defect in GaAs and Ga As 1 − x Sb x alloys," *Phys. Rev. B*, vol. 29, no. 8, pp. 4807–4810, Apr. 1984.

[11] H. J. Von Bardeleben, J. C. Bourgoin, and A. Miret, "Identification of the arsenic-antisite-arsenic-vacancy complex in electron-irradiated GaAs," *Phys. Rev. B*, vol. 34, no. 2, pp. 1360–1362, Jul. 1986.

[12] J. T. Schick, C. G. Morgan, and P. Papoulias, "First-principles study of As interstitials in GaAs: Convergence, relaxation, and formation energy," *Phys. Rev. B - Condens. Matter Mater. Phys.*, vol. 66, no. 19, pp. 1953021–19530210, Nov. 2002.

[13] S. Ganichev, E. Ziemann, W. Prettl, and I. Yassievich, "Distinction between the Poole-Frenkel and tunneling models of electric-field-stimulated carrier emission from deep levels in semiconductors," *Phys. Rev. B - Condens. Matter Mater. Phys.*, vol. 61, no. 15, pp. 10361–10365, Apr. 2000.

[14] J. Pienaar, W. E. Meyer, F. D. Auret, and S. M. M. Coelho, "Comparison of two models for phonon assisted tunneling field enhanced emission from defects in Ge measured by DLTS," in *Physica B: Condensed Matter*, 2012, vol. 407, no. 10, pp. 1641–1644.

[15] F. D. Auret and M. Nel, "Detection of minority-carrier defects by deep level transient spectroscopy using Schottky barrier diodes," *J. Appl. Phys.*, vol. 61, no. 7, pp. 2546–2549, Apr. 1987.

[16] F. D. Auret, R. M. Erasmus, S. A. Goodman, and W. E. Meyer, "Electronic and transformation

properties of a metastable defect introduced in n-type GaAs by $α$-particle irradiation," *Phys. Rev. B*, vol. 51, no. 24, p. 17521, Jun. 1995.

[17] F. Danie Auret, S. A. Goodman, and W. E. Meyer, "Electronic Properties and Introduction Kinetics of a Metastable Radiation Induced Defect in n-GaAs," *Mater. Sci. Forum*, vol. 196–201, pp. 1067–1072, 1995.

[18] S. D. Ganichev, W. Prettl, and I. N. Yassievich, "Deep impurity-center ionization by far-infrared radiation," *Phys. Solid State*, vol. 39, no. 11, pp. 1703–1726, Nov. 1997.

[19] A. Telia, B. Lepley, and C. Michel, "Experimental analysis of temperature dependence of deep-level capture cross-section properties at the Au oxidized InP interface," *J. Appl. Phys.*, vol. 69, no. 10, pp. 7159–7165, May 1991.

[20] V. Bondarenko, J. Gebauer, F. Redmann, and R. Krause-Rehberg, "Vacancy formation in GaAs under different equilibrium conditions," *Appl. Phys. Lett.*, vol. 87, no. 16, p. 161906, Oct. 2005.

[21] F. D. Auret, L. J. Bredell, G. Myburg, and W. O. Barnard, "Simultaneous observation of sub- and above threshold electron irradiation induced defects in gaas," *Jpn. J. Appl. Phys.*, vol. 30, no. 1, pp. 80–83, Jan. 1991.

[22] S. M. Tunhuma, F. D. Auret, M. J. Legodi, and M. Diale, "The fine structure of electron irradiation induced EL2-like defects in n -GaAs," *J. Appl. Phys.*, vol. 119, no. 14, p. 145705, Apr. 2016.

[23] F. D. Auret, M. Nel, and A. W. R. Leitch, "A DLTS analysis of electron and hole traps in VPE grown n-GaAs using schottky barrier diodes," *J. Electron. Mater.*, vol. 17, no. 2, pp. 111–113, Feb. 1988.

Figure captions

Figure 1. (a) Laplace DLTS spectra and (b) Conventional DLTS of three different carrier densities: 7.1×10^{14} $cm^{-3,}$ 1.9×10^{15} cm^{-3} and 1.0×10^{16} cm^{-3} doped n-GaAs. While conventional DLTS only detects one peak, Laplace DLTS is able to reveal the finer structure of the E3.

Figure 2. Arrhenius plot of the E3 in GaAs for 3 different carrier densities. The solid lines without symbols are for conventional DLTS scans. The subscripts beneath the E labels are the DLTS activation energies in eV determined from the Arrhenius plots. Note that the error bars for the E3b and E3c for the 7.1×10^{14} cm^{-3} are $\pm$ 0.01 because these defects are present in very low concentrations compared the defects in the 1.0×10^{16} cm^{-3} GaAs.

Figure 3. Concentration of the E3a in GaAs as a function of electron fluence from a ^{90}Sr radionuclide.

Figure 4. Laplace spectra of electron irradiated n-GaAs with four different carrier densities for three different types of spectra (as indicated in the figure). Spectra were recorded at a reverse bias of -2 V and a filling pulse amplitude of 2 V. The measurement temperature was 180 K.

Figure 5. Electric field dependence of E3a in GaAs for different free carrier densities.

Figure 6. (a) Electric field dependence of E3a in GaAs for different temperatures. (b) Tunneling time vs. 1000/T for the E3a. The equation of the regression line is shown in the legend.

Figure 7. Determination of the capture cross section of E3a in GaAs for $N_D = 1.9\times10^{15}$ cm^{-3} and $N_D = 1.0\times10^{16}$ cm^{-3}.

Figure 8. Arrhenius plot for the determination of the capture barrier of the E3a in a GaAs for $N_D = 1.9\times10^{15}$ cm^{-3} and $N_D = 1.0\times10^{16}$ cm^{-3}.

Figure 9. Isochronal annealing (10 min. periods) of the components of the E3 defect in GaAs, and the total E3 (square symbol) is the sum of the three E3 components.

Table Caption

Table I. Electronic properties of the E1-E2 defects and the E3 with its components in GaAs with a doping density of 1.9×10^{15} cm^{-3} and 1.0×10^{16} cm^{-3}.

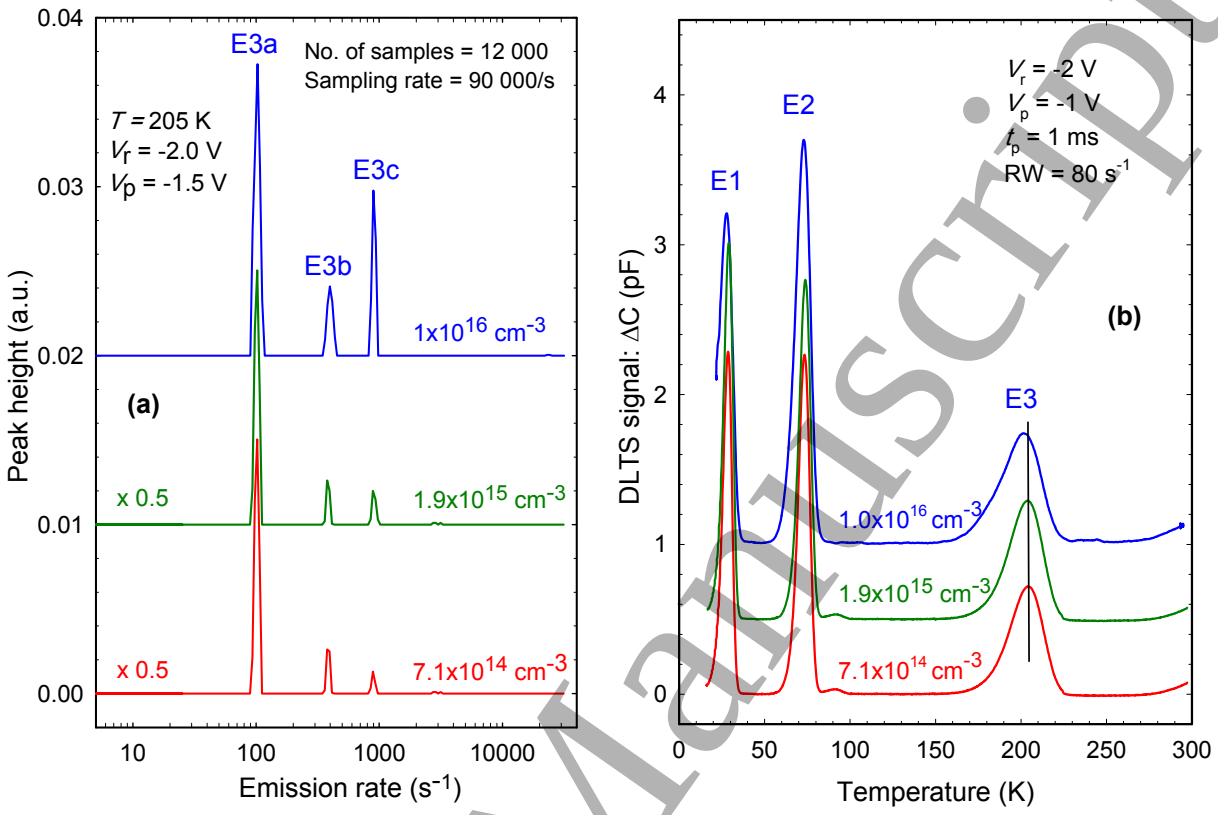

Figure 1 (of 9)

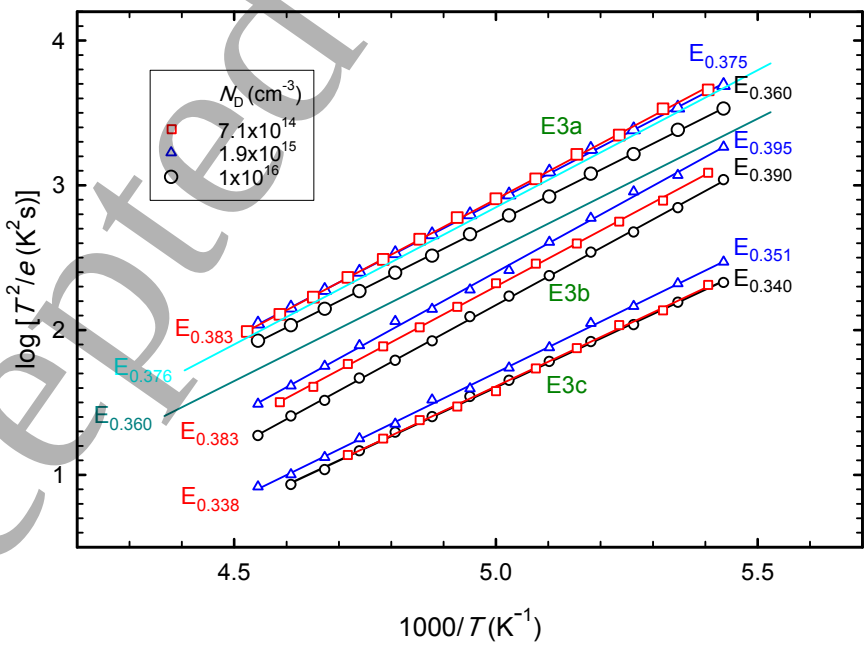

Figure 2 (of 9)

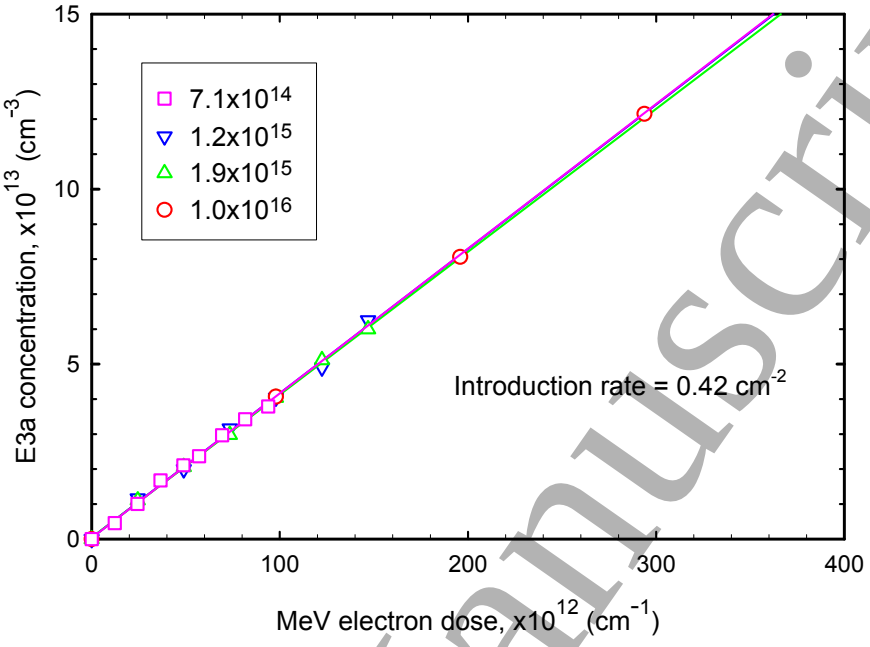

Figure 3 (of 9)

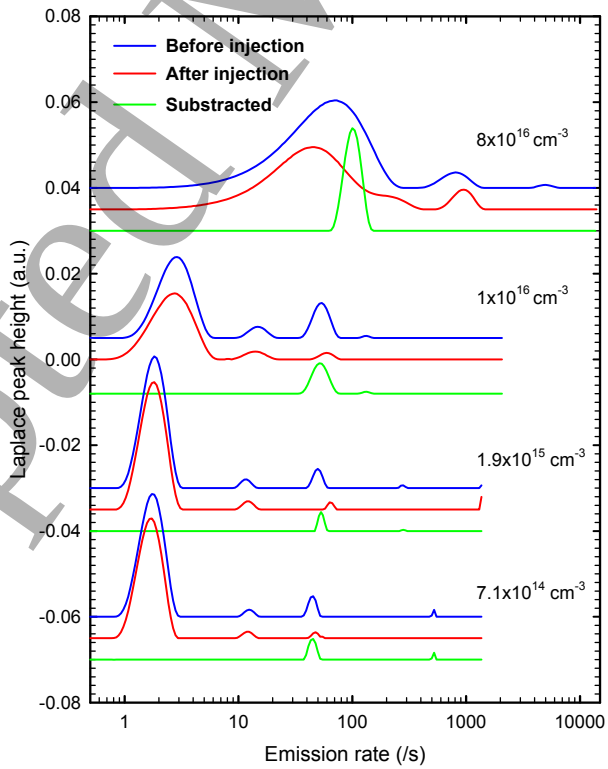

Figure 4 (of 9)

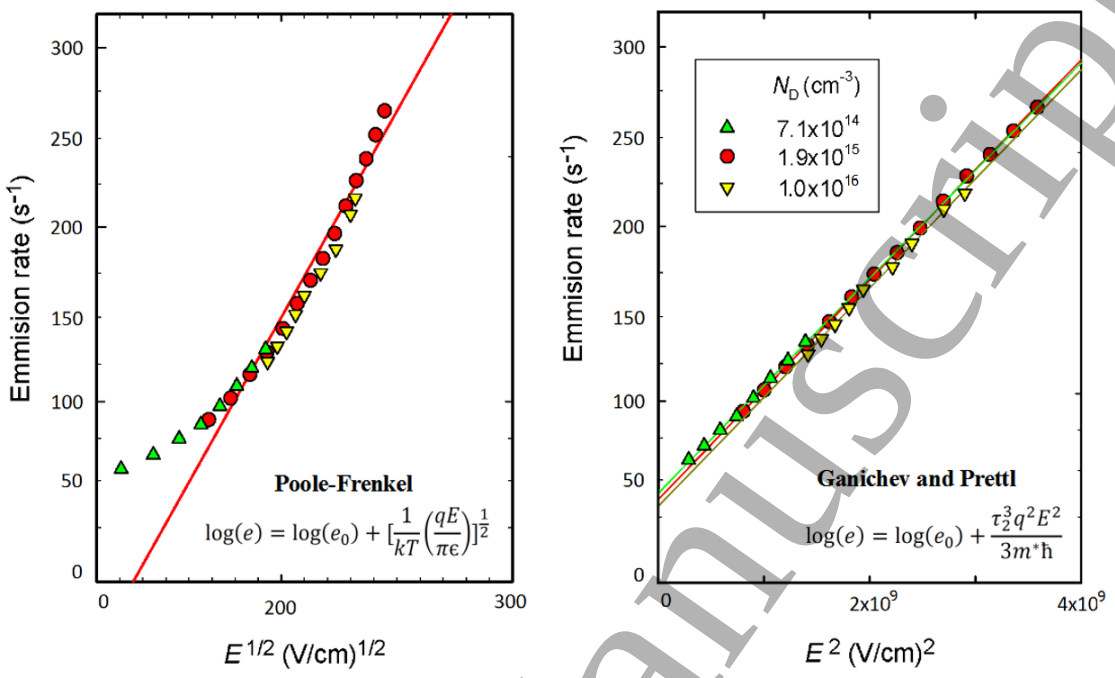

Figure 5 (of 9)

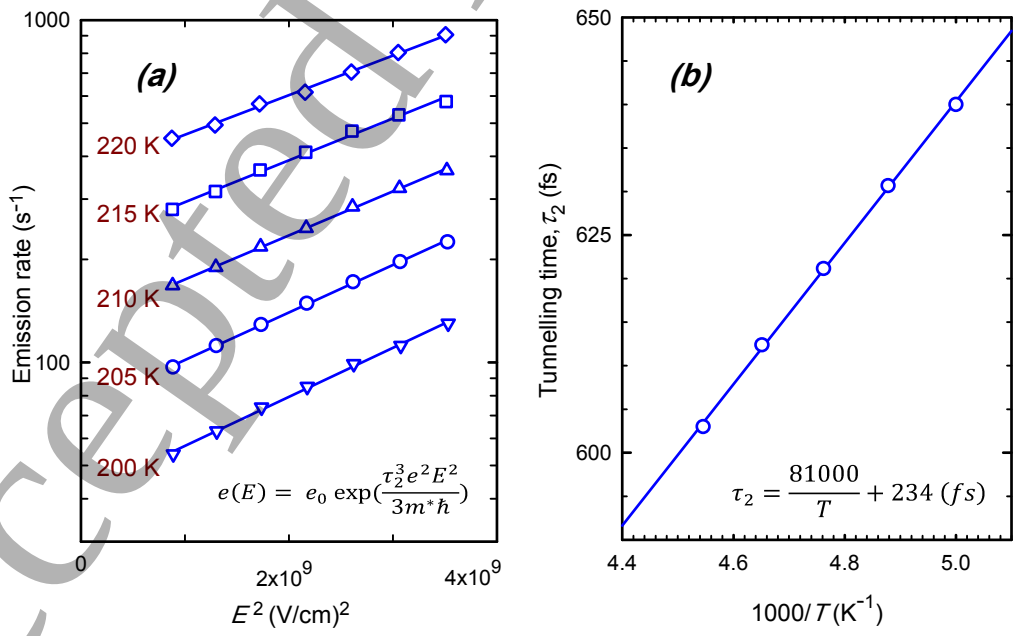

Figure 6 (of 9)

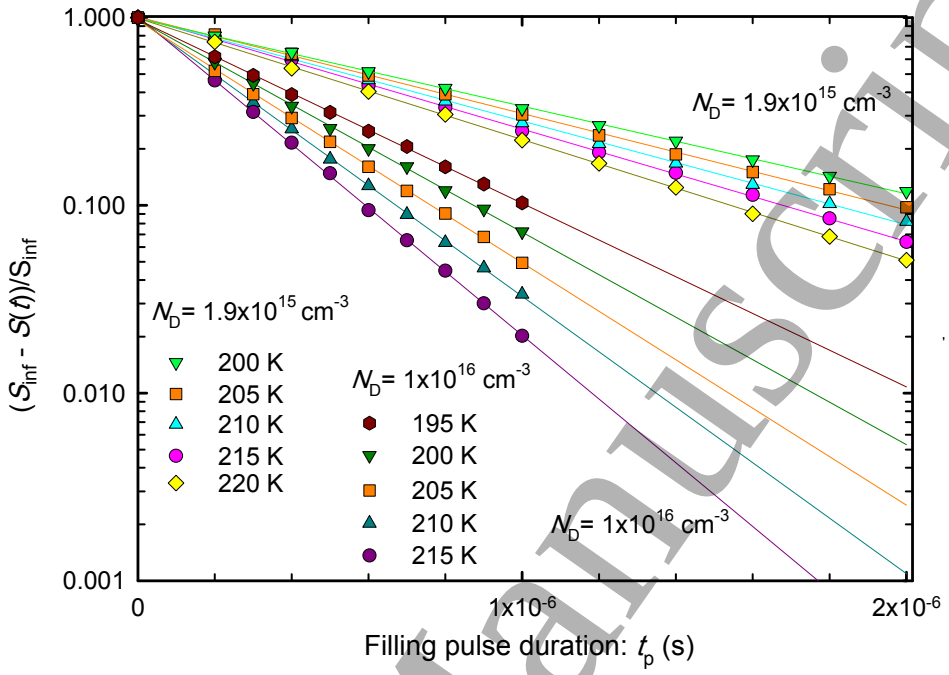

Figure 7 (of 9)

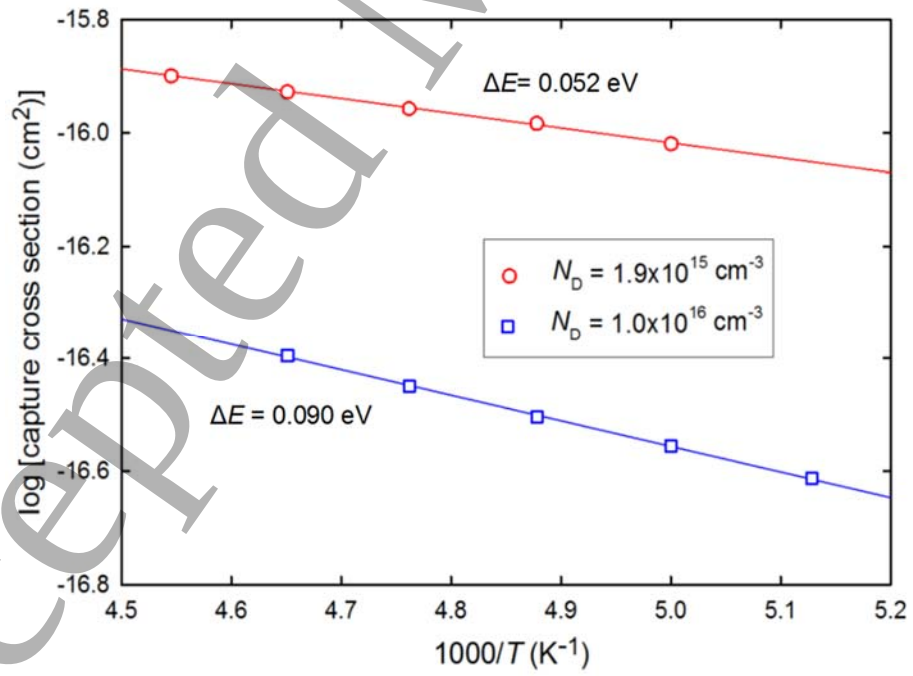

Figure 8 (of 9)

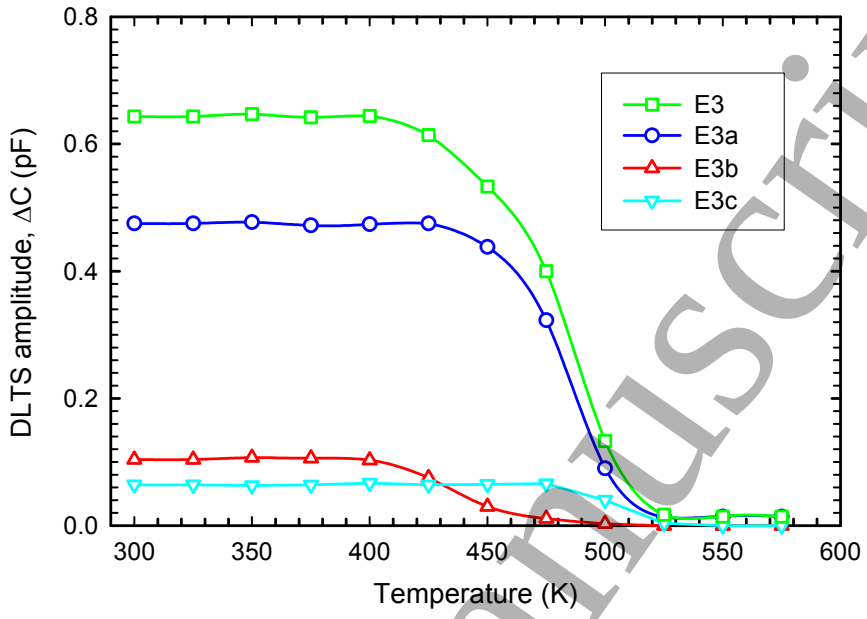

Figure 9 (of 9)

Defect	E_A (eV)	$\sigma_{n,a}$ (cm^2)	σ_n (cm^2)	Defect ID
E1	0.045	1.1×10^{-15} [21]	--------	Divacancy [9]
	0.040	1.6×10^{-17} [22]		
E2	0.142	1.3×10^{-13} [21]	--------	Divacancy [9]
	0.140	3.0×10^{-15} [22]		
E3	0.300 [7]	6.2×10^{-15} [7]	--------	-------
	0.375 [21]	1.3×10^{-14} [21]		
	0.390 [23]	6.0×10^{-14} [23]		
	$0.376^{\dagger}$	$4.1\times10^{-14\dagger}$		
	0.360^{*}	$3.2\times10^{-14\,*}$		
E3a	0.380”	4.7×10^{-14}”	3.0×10^{-16} ” (205K)	V_{As}
	$0.375^{\dagger}$	$2.9\times10^{-14\,\dagger}$	1.0×10^{-16} † (205K)	
	0.360^{*}	$2.1\times10^{-14\,*}$	3.1×10^{-17} * (205 K)	
E3b	0.383”	2.1×10^{-13}”	----------	As_i
	$0.395^{\dagger}$	$3.4\times10^{-13\,\dagger}$		
	0.390^{*}	$4.8\times10^{-13*}$		
E3c	0.338”	7.7×10^{-14}”	----------	V_{Ga}-Si_{Ga}
	$0.351^{\dagger}$	$1.3\times10^{-13\,\dagger}$		
	0.340^{*}	$6.8\times10^{-14*}$		

”This study, measured in material with a free carrier density of 7.1×10^{14} cm^{-3}

†This study, measured in material with a free carrier density of 1.9×10^{15} cm^{-3}

*This study, measured in material with a free carrier density of 1.0×10^{16} cm^{-3}

Table I